J|A|C|S
ARTICLES

Published on Web 07/08/2010

Diferrocenyl Molecular Wires. The Role of Heteroatom Linkers

Yu Li, Mira Josowicz, and Laren M. Tolbert*

School of Chemistry and Biochemistry, Georgia Institute of Technology, 901 Atlantic Drive, Atlanta, Georgia 30332-0400

Received March 4, 2010; E-mail: laren.tolbert@chemistry.gatech.edu

Abstract: Diferrocenyl molecular "wires", in which two ferrocenes are linked by a conjugated chain, allowing the communication of redox information between the ferrocenes, are a versatile platform on which to investigate notions of molecular conductivity. In this paper, we examine the role of heteroatoms—including O, P, S, and Se, as well as C atoms in various oxidation states—separated from the ferrocenes by intervening double bonds which minimize any steric effects. Surprisingly, oxygen is a better electronic mediator than sulfur, a phenomenon we attribute to superior molecular orbital overlap. These fundamental studies on redox coupling will help to guide the design of efficient organic conductors for organic electronics.

Introduction

The notion of molecular "wires" has captured the imagination of chemists and physicists in semiconductor nanotechnology.[1] Missing are clear concepts of what this term means and how it relates to structure and function. Although such wires are often portrayed as single conductive paths, and the measurement of single-molecule conductance has emerged as a rich and provocative research area, most often such wires are used in ensembles connecting metallic surfaces.[2] Moreover, such wires often possess a low-dimensional π-conjugation backbone that can carry electrons through a distance of several nanometers.[3] Directly addressing the conductivity of a distinct molecule, for instance, by assembling an electronic junction connected by the molecular wire, is still fraught with problems. Therefore, an indirect approach with a donor−bridge−acceptor motif remains the most useful prototype for examining the capability of a single molecule to support charge transfer. Molecules of this kind must not only satisfy the dimensional requirements but also have the appropriate electronic properties.

Electron transport across molecules is generally divided into two alternative types: *superexchange* and *hopping*. In the superexchange mechanism,[4] the donor and acceptor orbitals are assumed to overlap with the highest occupied molecular orbital (HOMO) and lowest unoccupied molecular orbital (LUMO) of the bridging group, while the direct orbital overlaps between the donor and acceptor are negligible. Thus, the coupling between donor and acceptor is furnished by indirect mixing of the donor and acceptor wave functions through the mediation of the bridging component. The efficiency of such a mechanism is determined by the effective overlap between donor and acceptor. In the hopping mechanism, the electron (or hole) transiently resides on the midway bridging group so that a chemical intermediate is generated. Early efforts commonly have treated them separately, but recent research has also shown that both mechanisms can function simultaneously.[5]

Ferrocenes are ideal donor moieties, since, unlike conventional aromatics, the HOMO is localized not in the π system but in a metal-centered d orbital.[6] In addition, the ease of organic functionalization, the chemical stability of the neutral and charged species, the low oxidation potential to allow effective coupling with the organic component, and the diamagnetism in the neutral state (thus enabling NMR characterization) make ferrocenes one of the most employed candidates in implementing the wire-bridged complex and for studying electronic communication.[7] The mixed valence (MV) state of the biferrocenyl complex is of the most interest, since the charge mobility in this system can be directly characterized by electrochemistry, structural analysis, electronic spectroscopy, ESR, Mössbauer, etc. We note in this regard that our studies are complementary to previous studies in which electronic coupling between carbene and nitrene centers is mediated by a chalcogenide.[8]

Previously we have shown that a solitonic bridge, i.e., a polyenyl cation or anion, maintains electrical communication

(1) (a) Chen, F.; Tao, N. J. *Acc. Chem. Res.* **2009**, *42*, 429–438. (b) Wang, C.; Plsson, L.-O.; Batsanov, A. S.; Bryce, M. R. *J. Am. Chem. Soc.* **2006**, *128*, 3789–3799. (c) Flores-Torres, S.; Hutchison, G. R.; Soltzberg, L. J.; Abruña, H. D. *J. Am. Chem. Soc.* **2006**, *128*, 1513–1522.

(2) (a) Chen, J.; Reed, M. A.; Asplund, C. L.; Cassell, A. M.; Myrick, M. L.; Rawlett, A. M.; Tour, J. M.; Van Patten, P. G. *Appl. Phys. Lett.* **1999**, *75*, 624–626. (b) Carroll, R. L.; Gorman, C. B. *Angew. Chem., Int. Ed.* **2002**, *41*, 4378–4400. (c) Metzger, R. M. *Chem. Rev.* **2003**, *103*, 3803–3834.

(3) Sikes, H. D.; Smalley, J. F.; Dudek, S. P.; Cook, A. R.; Newton, M. D.; Chidsey, C. E. D.; Feldberg, S. W. *Science* **2001**, *291*, 1519–1523.

(4) (a) Anderson, P. W. *Phys. Rev.* **1959**, *115*, 2–13. (b) Marcus, R. A. *J. Chem. Phys.* **1965**, *43*, 679–701.

(5) (a) Petrov, E. G.; May, V. *J. Phys. Chem. A* **2001**, *105*, 10176–10186. (b) Sim, E. *J. Phys. Chem. B* **2004**, *108*, 19093–19093. (c) Weiss, E. A.; Ahrens, M. J.; Sinks, L. E.; Gusev, A. V.; Ratner, M. A.; Wasielewski, M. R. *J. Am. Chem. Soc.* **2004**, *126*, 5577–5584.

(6) Boccia, A.; Marrani, A. G.; Stranges, S.; Zanoni, R.; Alagia, M.; Cossi, M.; Iozzi, M. F. *J. Chem. Phys.* **2008**, *128*, 154315/1–154315/9.

(7) Sundararaman, A.; Venkatasubbaiah, K.; Victor, M.; Zakharov, L. N.; Rheingold, A. L.; Jaekle, F. *J. Am. Chem. Soc.* **2006**, *128*, 16554–16565.

(8) (a) Matsuda, K.; Yamagata, T.; Seta, T.; Iwamura, H.; Hori, K. *J. Am. Chem. Soc.* **1997**, *119*, 8058–8064. (b) Minato, M.; Lahti, P. M. *J. Phys. Org. Chem.* **1994**, *7*, 495–502. (c) Itoh, K.; Takui, T.; Teki, Y.; Kinoshita, T. *Mol. Cryst. Liq. Cryst.* **1989**, *176*, 49–66. (d) Nimura, S.; Kikuchi, O.; Ohana, T.; Yabe, A.; Kaise, M. *Chem. Lett.* **1994**, *9*, 1679–82.

10.1021/ja101585z

up to 13 carbon atoms.[9] However, the use of such bridges is complicated by the ionic nature of the substrates. In contrast, it has been very common to use a number of heteroatoms (silicon, phosphorus, or sulfur) to bind redox-active surfaces. In this case, the pair of electrons on the heteroatom serves to substitute for the more mobile electron pair (or hole) within a soliton. Little discussion, however, has taken place over the nature of the conduction path. How well do such linking groups facilitate or block electronic communication? In this study we seek to establish the nature of that charge transport.

If we compare a diferrocenyl "soliton" molecule $(Fc\text{-}(CH)_5Fc)^-$ with an isoelectronic molecule containing a heteroatom (FcCH═CHXCH═CHFc), we see that the HOMO has a striking similarity to that for the solitonic molecule. However, the redox potential of the replacement group would be expected to have a profound effect, as would the polarizability of the substituted group. We were concerned that the rather naïve views of resonance extant in the community lead to the assumption that resonance is equally effective whether through a double bond, a triple bond, heteroatom, an aromatic ring, or a heteroaromatic ring. Since the range of molecules studied by various methods does not allow ready comparison, we determined to compare a range of molecules of type FcCH═CHXCH═CHFc, in which the group X was varied across the common range of linking groups studied but for which the vinylene groups CH═CH served to minimize steric effects which would otherwise intervene.

In examining the capability of the bridging moiety −CH═CHXCH═CH− in supporting intramolecular electronic interactions, our methods involve electrochemistry and near-infrared (near-IR) absorption spectroscopy of the mixed-valence species. If we consider a bis-ferrocenyl molecule for which the connecting bridge is insulating, then the half-wave potential of each ferrocene is the same, save for an entropy effect,[10] and we observe a single two-electron wave. Conversely, an effective bridge alters the second half-wave potential, and the difference between the two potentials is an indication of the effectiveness of the wire. In addition, intervalence electron transfer can be detected and quantitatively studied from the characteristics of the intervalence band of mixed-valence complexes. Basically, the intervalence transition is considered as a special case of charge transfer transition, the reduced site (Red) being the donor group, while the oxidized site (Ox) is the acceptor group. The mixing of the two electronic states Red-Ox and Ox-Red is due to the electronic coupling term V_{ab}, which is also responsible for the intensity of the intervalence transition. Thus, V_{ab} and the derived delocalization parameter α can be determined by the following formulas[11] according to Hush's theoretical treatment:

$$V_{ab} = (2.05 \times 10^{-2})(V_{max}\varepsilon_{max}\Delta\upsilon_{1/2})^{1/2}/R_{MM} \quad (1)$$

$$\alpha = V_{ab}/\nu_{max} \quad (2)$$

where V_{ab} is the coupling (cm^{-1}), ε_{max} is the maximum extinction coefficient, ν_{max} is the band position (cm^{-1}), $\Delta\nu_{1/2}$ is the full width at half-maximum (cm^{-1}), and R_{MM} is the metal−metal distance (Å).

Scheme 1. Mechanism of Charge Injection and Propagation in Diferrocenyl Chalcogenides

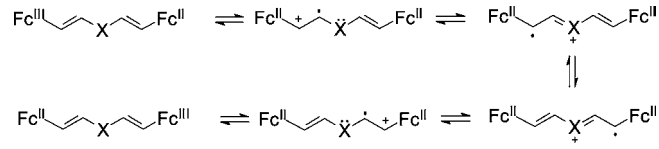

As stated earlier, the effectiveness of organic wires using the prototype binuclear complexes largely relies on efficient coupling between the d orbital of the metal and the frontier p orbital of the bridging fragment. We expect that electron transfer from one metal to another will be more efficient when the energy gap between the metal orbital and organic fragment is narrowed to allow enhanced charge delocalization. In the present series, the X group, in one sense, serves to tune the relevant energy levels (Scheme 1).

The subjects of our study are represented by the general formula FcCH═CHXCH═CHFc (**1-X**), with X representing the common range of linking groups used either to attach directly to an electrode or between delocalized moieties. These consist of X = S (**1-S**), O (**1-O**) Se (**1-Se**), CH_2 (**1-CH$_2$**), $(CH_2)_2$ (**1-C$_2$H$_4$**), C≡C (**1-C$_2$**), CH═CH (**1-C$_2$H$_2$**), PPh (**1-PPh**), P(═O)Ph (**1-POPh**), P(═S)Ph (**1-PSPh**), C═O (**1-CO**), CH^+ (**1-CH$^+$**), "none" (**1-Ø**; i.e., 1,4-diferrocenyl-1,3-butadiene) (see Figure 1).

Results

Synthesis. The systems described below were synthesized by a combination of Wittig (route A) and Horner−Emmons−Wadsworth (HEW, route B) coupling reactions (Figure 2). Initial syntheses with the Wittig approach produced mixtures of cis and trans isomers, due to the nonstereoselectivity of the conventional Wittig reaction, while the HEW approach produced the trans isomers exclusively, as indicated by single-crystal X-ray diffraction.[12] Thus, assignment of the stereochemistry was made straightforwardly by analysis of the NMR coupling constants ($J_{trans} \approx 15$ Hz, $J_{cis} \approx 11$ Hz) and confirmation by the X-ray data of the crystallized samples.

Addition of 2 equiv of ferrocenecarboxaldehyde (FcCHO) to the bis(ylide) of the appropriate bis(triphenylphosphoniummethyl)-X dibromide, i.e., $(BrPh_3P^+CH_2)_2X\cdot Br^-_2$, produced a number of the desired compounds with reasonable yields (X = CH_2, $(CH_2)_2$, C_2H_2, S, O). In each case, a mixture of cis (*Z*) and trans (*E*) isomers was obtained, as evidenced by NMR spectroscopy. Separation of the isomers by column chromatography or recrystallization proved very difficult and was only partially successful for some of the compounds.

In contrast, the Horner−Wadsworth−Emmons (HEW) reaction[13] stereospecifically produced (*E*)-alkenes. In general, the synthetic precursors, bis(diethylphosphinylmethylene) derivatives ($[(EtO)_2P(O)CH_2]_2X$), were prepared through the Arbuzov reaction by refluxing a dibromide with triethyl phosphite. In the HEW olefination step, heating was essential to allow the reaction to proceed and to promote generation of double bonds in *E* form.

When the X group was a heteroatom such as S or Se, the HEW reactions proceeded smoothly at room temperature but

(9) Tolbert, L. M.; Zhao, X. *J. Am. Chem. Soc.* **1997**, *119*, 3253–3258.
(10) For an extended discussion, see: Flanagan, J. B.; Margel, S.; Bard, A. J.; Anson, F. C. *J. Am. Chem. Soc.* **1978**, *100*, 4248–4253.
(11) (a) Hush, N. S. *Coord. Chem. Rev.* **1985**, *64*, 135–57. (b) Hush, N. S. *Prog. Inorg. Chem.* **1967**, *8*, 391–444.
(12) Unless specifically indicated, the absence of stereochemical prefixes means that the compounds were a mixture of *E,E* and *E,Z* isomers.
(13) (a) Horner, L.; Hoffmann, H. M. R.; Wippel, H. G. *Ber. Bunsen-Ges. Phys. Chem.* **1958**, *91*, 61–63. (b) Wadsworth, W. S., Jr.; Emmons, W. D. *J. Am. Chem. Soc.* **1961**, *83*, 1733–1738.

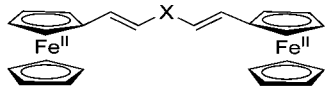

1-S, X = S
1-O, X = O
1-Se, X = Se
1-CH$_2$, X = CH$_2$
1-C$_2$H$_4$, X = CH$_2$CH$_2$
1-C$_2$, X = C≡C
1-C$_2$H$_2$, X = CH=CH
1-PPh, X = PPh
1-POPh, X = P(=O)Ph
1-PSPh, X = P(=S)Ph
1-CO, X = C=O
1-CH$^+$, X = CH$^+$
1-Ø, X = "-"

Figure 1. Ferrocenes used in this study.

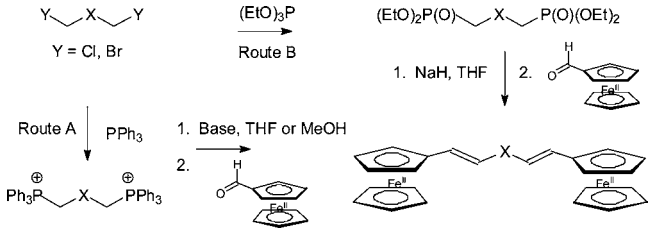

Figure 2. Synthesis of FcCH=CHXCH=CHFc.

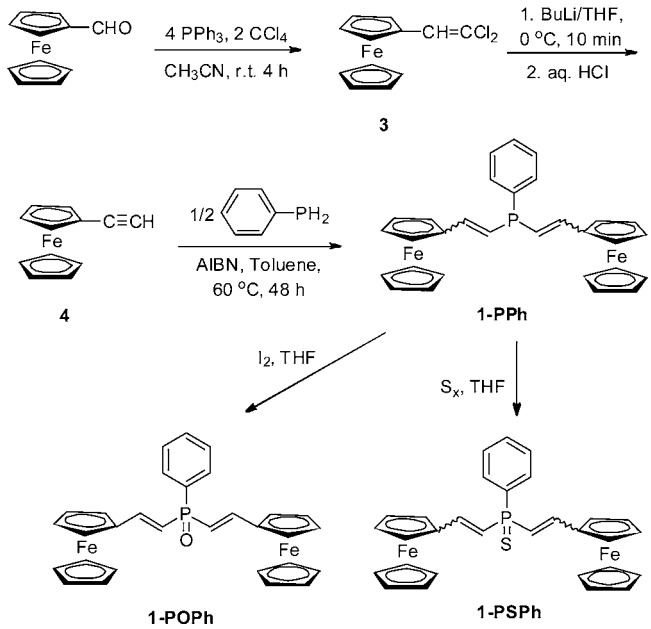

Figure 3. Synthesis of **1-PPh**, **1-PSPh**, and **1-POPh**.

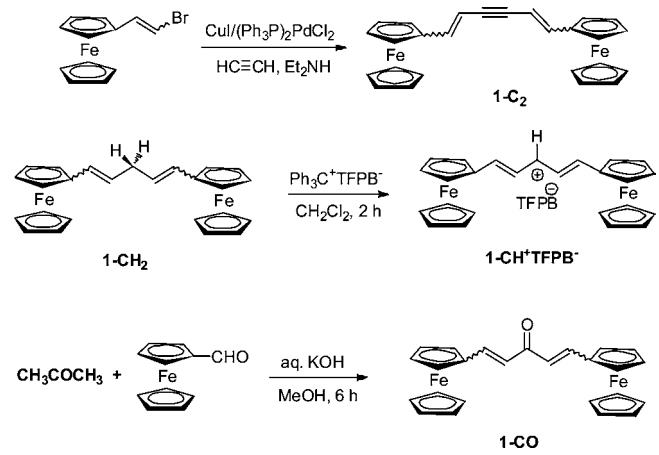

Figure 4. Synthesis of **1-C$_2$**, **1-CH$^+$**, and **1-CO**.

only afforded an improved *E*,*E* stereochemistry (approximately 70%) in comparison with the corresponding Wittig reactions. When the same reactions were conducted under reflux, however, nearly 95% *E*,*E* adduct was observed, as evidenced by ^{1}H NMR spectroscopy. The pure *E*,*E* isomer could be conveniently isolated by recrystallization from CH_2Cl_2/hexane (1:1). Our efforts to use HEW reactions for the remaining compounds to achieve exclusive *E*,*E* product were unsuccessful.

The preparation of the phosphorus-substituted ferrocenes used a modification of Kobayashi's procedure (Figure 3).[14] Phenylphosphine was added to 2 equiv of ethynylferrocene[15] to give the double 1:2 adduct **1-PPh** in high yield. The ^{1}H NMR spectrum of the isolated product showed predominantly trans vinylene protons with minor cis vinylene contributions. Stirring this phenylphosphine derivative with excessive elemental sulfur in THF under argon furnished the phenylphosphine sulfide **1-PSPh** in high yield (Figure 3). The phosphine oxide **1-POPh** was conveniently obtained by the treatment of **1-PPh** with 1 equiv of iodine and a trace of water in THF. These two transformations could be easily observed by ^{1}H NMR spectroscopy, in which the para phenyl proton was noticeably shifted to low field upon oxygenation or thionylation. Interestingly, whereas the stereochemistry of **1-PSPh** basically inherited that of the antecedent compound **1-PPh**, **1-POPh** was produced exclusively as the *E*,*E* adduct (see Figure 3).

Bis(2-ferrocenyl)hexa-1,5-dien-3-yne (**1-C$_2$**) was prepared through a modified Stephans−Castro reaction[16] (Figure 4). (1-Bromovinyl)ferrocene (FcCH=CHBr) was first prepared via Wittig coupling of (bromomethyl)triphenylphosphonium bromide[17] with ferrocenecarboxaldehyde.[18] Cuprous iodide was added to a mixture of bis(triphenylphosphine)palladium dichloride and a diethylamine solution of FcCH=CHBr under an inert atmosphere followed by passing a slow current of acetylene gas. After workup and column chromatography, the symmetrical disubstituted acetylene **1-C$_2$** was obtained as a bright red solid in very good yield (85%). The final product was characterized by ^{1}H NMR spectroscopy as a mixture of *E* and *Z* isomers. Finally, **1-CH$^+$BArF$^-$** was prepared as described previously for the tetrafluoroborate salt **1-CH$^+$BF$_4^-$**.[19]

Whereas most of the bis(2-ferrocenylvinyl) compounds prepared here were fairly stable both in the solid/liquid state and in solution, there were a few exceptions. Fc(CH=CH)$_2$Fc (**1-Ø**) and Fc(CH=CH)$_3$Fc (**1-C$_2$H$_2$**) were observed to have low stability in solution. An unknown brick red solid was isolated from solution after standing, which has been reported by

(14) Kobayashi, E.; Obata, T.; Asohima, S.; Furukawa, J. *Polym. J.* **1993**, *25*, 1049–1057.
(15) Luo, S. J.; Liu, Y. H.; Liu, C. M.; Liang, Y. M.; Ma, Y. X. *Synth. Commun.* **2000**, *30*, 1569–1572.
(16) (a) Sonogashira, K.; Tohda, Y.; N. H., *Tetrahedron Lett.* **1975**, 4467–4470. (b) Stephens, R. D.; Castro, C. E. *J. Org. Chem.* **1963**, *28*, 3313–3315.
(17) Driscoll, J. S.; Grisley, D. W.; Pustinger, J. V.; Harris, J. E.; Matthews, C. N. *J. Org. Chem.* **1964**, *29*, 2427–2431.
(18) Barlow, S.; Henling, L. M.; Day, M. W.; Schaefer, W. P.; Green, J. C.; Hascall, T.; Marder, S. R. *J. Am. Chem. Soc.* **2002**, *124*, 6285–6296.
(19) See: Zhao, X. Ph.D. Thesis, Georgia Institute of Technology, 1996 and the Supporting Information.

Spangler as being due to decomposition or polymerization.[20] Thus, during purification procedures, fast recrystallization or flash chromatography was always performed.

As discussed, some of the compounds were obtained as *E,Z* isomeric mixtures. For instance, **1-C$_2$**, **1-PPh**, and **1-Ø** contained all three configurational isomers, as evidenced by NMR spectroscopy. The initial Wittig approach almost always afforded *E,Z* isomeric mixtures, even though the *E,E* isomer was the major component. Efforts to separate the isomers by slow chromatography or recrystallization turned out to be either extremely tedious or fruitless. Attempted isomerization to the thermodynamically more stable products using conventional methods, e.g., catalytic amounts of I_2 or *p*-toluenesulfonic acid led to decomposition. However, the presence of both *E,Z* mixtures (Wittig) and *E,E* mixtures (HEW) allowed us to unambiguously assign stereochemistry and compare the properties of pure isomers with those of the mixtures (see below). In all cases, the electrochemical and spectroscopic properties were indistinguishable. Additionally, our earlier study[9] on the diferrocenyl complex bridged by a polymethine cation has revealed that the synthetic precursor **1-CH$_2$**, a geometric mixture, was converted to the thermodynamically favorable *E,E* cationic form upon hydride extraction as shown:

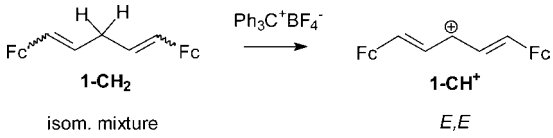

Electrochemistry. Previous cyclic voltammetric studies in our laboratory used conventional $Bu_4N^+PF_6^-$, BF_4^-, or ClO_4^- as the supporting electrolyte.[9] More recently, the use of less nucleophilic counterions, $B(C_6F_5)_4^-$ and $B[3,5\text{-}C_6H_3(CF_3)_2]_4^-$ ($BArF^-$), has been found to give wider peak separations than the conventional anions.[21,22] The improved electrochemistry arises from the weakly coordinating nature of the bulky anions.[23] Geiger and co-workers have performed extensive studies on the fluoroarylborate anions; the reported larger peak separation was ascribed to the low ion-pairing effect.[24] In our hands, the $BArF^-$ anion provided improved solubility and enhanced peak separations and was used for all the electrochemistry in this study.

As an example of the counterion effect, **1-S** exhibited a single two-electron oxidation wave (−50 mV vs Fc/Fc^+) in a solution of $Bu_4N^+PF_6^-$ in CH_2Cl_2 but two well-separated one-electron waves (ΔE = 180 mV) when the supporting electrolyte was $Bu_4N^+BArF^-$ (see Figure 5). For these reasons, we selected $Bu_4N^+BArF^-$ and the oxidatively more stable solvent CH_2Cl_2 as the electrochemical media throughout this work. The synthetic precursor Na^+BArF^- was easily prepared from commercially available 3,5-bis(trifluoromethyl)bromobenzene via a multiple-step one-pot reaction in 90% yield.[25] Ion metathesis of

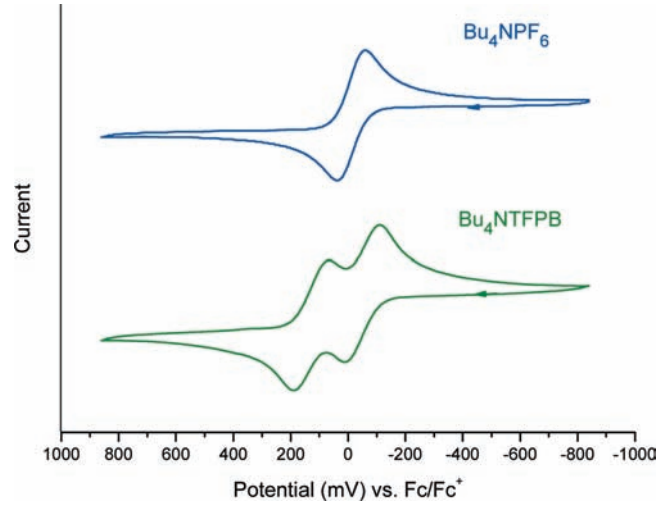

Figure 5. Cyclic voltammograms of **1-S** in a CH_2Cl_2 solution with $Bu_4N^+PF_6^-$ (top) or $Bu_4N^+BArF^-$ (bottom) as supporting electrolyte. Scan rate: 50 mV/s.

Na^+BArF^- with $Bu_4N^+Br^-$ readily afforded the electrolyte $Bu_4N^+BArF^-$. This ammonium salt was recrystallized several times from CH_2Cl_2/Et_2O and passed through an alumina column (CH_2Cl_2) prior to use.

In performing the electrochemistry, our major concern was whether the stereochemistry would affect the electrochemical behavior, leading to incorrect conclusions. Fortunately, the use of both Wittig and HEW methodologies provided more than five bis(ferrocenylvinyl) compounds as both isomeric mixtures and *E,E* products. Furthermore, we also made both (*E,E,E*)- and (*E,Z,E*)-**1-C$_2$H$_2$**. With this sample library at hand, we were able to conduct comparative studies of the impact of stereochemistry on the corresponding electrochemical behaviors. No electrochemical variations with the steric arrangement of the double bonds were observed.[26]

An obvious question which arose from this lack of dependence on stereochemistry was whether this reflected the underlying electronics or simply an electron-transfer-mediated isomerization during the cathodic process. To test this, a small amount of the isomeric mixture of **1-S** under an argon atmosphere was first electrochemically exposed to a constant potential 200 mV positive of the second oxidation wave of **1-S**. The brown solution was immediately exposed to a constant potential 400 mV negative of the first oxidation potential. After column chromatography, almost 90% of **1-S** was recovered. The NMR of the isolated product indicated exclusive formation of the *E,E* form (see Figure 6).

With these controls in place, we obtained the polarographic first and second oxidation potentials of all compounds **1-X** and report them in Table 1, using the Fc/Fc^+ couple as reference. This simplest member of the series, X = CH_2 (**1-CH$_2$**), showed a peak separation of 115 mV which disappeared upon extension to X = CH_2CH_2 (**1-C$_2$H$_4$**). In contrast, use of the triple bond C≡C (**1-C$_2$**) as the connecting group led to a diminution of the coupling relative to CH═CH (**1-C$_2$H$_2$**). Similarly, and surprisingly, in the chalcogenide series O, S, and Se, oxygen was most effective in maintaining conjugation, despite its higher oxidation potential. Conversely, the electron-poor carbonyl chain (X = CO, **1-CO**) actually produced an effective bridge. Moreover,

(20) Ribou, A.-C.; Launay, J.-P.; Sachtleben, M. L.; Li, H.; Spangler, C. W. *Inorg. Chem.* **1996**, *35*, 3735–3740.
(21) Barrière, F.; Camire, N.; Geiger, W. E.; Mueller-Westerhoff, U. T.; Sanders, R. *J. Am. Chem. Soc.* **2002**, *124*, 7262–7263. (b) LeSuer, R. J.; Geiger, W. E. *Angew. Chem., Int. Ed.* **2000**, *112*, 254–256.
(22) Olson, E. J.; Boswell, P. G.; Givot, B. L.; Yao, L. J.; Buehlmann, P. *J. Electroanal. Chem.* **2010**, *639*, 154–160.
(23) Strauss, S. H. *Chem. Rev.* **1993**, *93*, 927–942.
(24) (a) Camire, N.; Mueller-Westerhoff, U. T.; Geiger, W. E. *J. Organomet. Chem.* **2001**, *637−639*, 823–826. (b) Barriere, F.; Geiger, W. E. *J. Am. Chem. Soc.* **2006**, *128*, 3980–3989.
(25) (a) Reger, D. L.; Wright, T. D.; Little, C. A.; Lamba, J. J. S.; Smith, M. D. *Inorg. Chem.* **2001**, *40*, 3810–3814. (b) Bahr, S. R.; Boudjouk, P. *J. Org. Chem.* **1992**, *57*, 5545–5547.

(26) A lone exception was when X was *o*-phenylene. This "exception which proves the rule" will be discussed in a future paper.

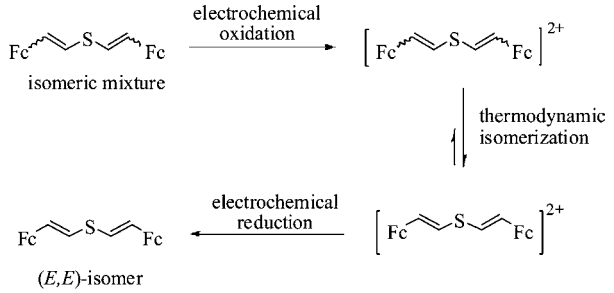

Figure 6. Electrochemical isomerization/equilibration of **1-S.**

Table 1. Electrochemical Data[a,b] (from Cyclic Voltammetry) for Compounds **1-X**

1-X	X	E_1, mV	E_2, mV	ΔE, mV	K_c
1-Ø	none	−35	190	225	6300
1-C_2H_2	CH═CH	−80	100	180	1100
1-CH^+	CH^+	−75	210[c]	285[b]	65100
1-C_2	C≡C	50	175	125	130
1-CH_2	CH_2	−25	90	115	88
1-C_2H_4	CH_2CH_2	0	0	0	
1-CO	C═O	+110	235	125	130
1-O	O	−90	110	200	2400
1-S	S	−50	130	180	1100
1-Se	Se	+50	125	75	19
1-PPh	PPh	−20	160[b]	180[b]	1100[b]
1-PSPh	P(S)Ph	+60	210	150	340
1-POPh	P(O)Ph	+140	240	100	50

[a] Conditions: electrolyte, $Bu_4N^+BArF^-$ (0.1 M); working electrode, Pt; reference electrode, Ag/AgI, corrected to Fc; scan rate, 50 mV/s. [b] Relative to Fc. [c] Irreversible oxidation wave.

due to the lack of reversible oxidation waves, we exclude **1-PPh** from further discussion.

Using the equilibrium [Fc-B-Fc] + $[Fc\text{-}B\text{-}Fc]^{2+}$ ⇌ 2 $[Fc\text{-}B\text{-}Fc]^+$, we were able to calculate the conproportionation constant K_c for the radical cations in each case. These are also entered in Table 1.

Spectroscopy. In order to achieve partially oxidized substrates to compare with our electrochemical results, we found chemical oxidation to be more convenient, to be easier to manipulate, and to provide more reproducible results. Thus, we adapted this method for all the mixed-valence absorption studies, using the data provided by Connelly and Geiger.[27] We determined that $Fc^+PF_6^-$ and $Ar_3N^{\bullet+}SbCl_6^-$ (TBA or "magic blue," Ar = *p*-BrC_6H_4) were very good oxidation reagents for the diferrocenyl compounds, especially $Fc^+PF_6^-$. The mild oxidation strength of $Fc^+PF_6^-$ (0.0 V vs Fc/Fc^+) would oxidize the first ferrocene moiety but not the second one for most compounds, which had a negatively shifted first oxidation and a higher second oxidation potential than the Fc/Fc^+ couple. When a stronger oxidant was required, TBA was used (0.76 V vs Fc/Fc^+). It is noteworthy that both the oxidants and their reduced forms did not have absorptions in the low-energy region which could have interfered with the mixed-valence spectra. The general procedure is described in the Supporting Information. For weak coupling compounds, 0.1−1.0 equiv of oxidant was used to minimize the possible disproportionation. $Fc^+PF_6^-$ absorbs at ca. 622 nm with an extinction coefficient of 374 cm^{-1} M^{-1},[28] which is essentially negligible compared to the absorption of the ferrocenium moiety of the mixed-valence species herein and the low-energy absorptions in the near-IR region.

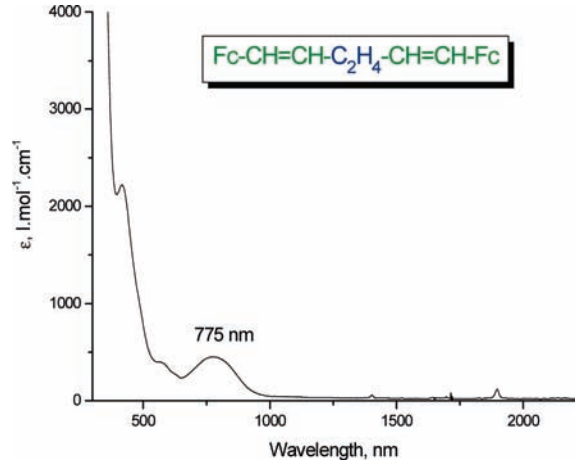

Figure 7. Spectrum of the radical cation of **1-C_2H_4**.

The mixed-valence spectra of bis-ferrocene compounds are often complicated by the overlapping of the coexisting absorptions arising from different types of electronic transitions in the low-energy area. This is especially the case for the current mixed-valence species herein due to the large variety of the bridging ligands CH═CHXCH═CH employed. Therefore, spectral deconvolution in the frequency mode is generally required to resolve the discrete bands into Gaussian components. Such curve fittings were conveniently fulfilled with the Origin peak fitting module (PFM).[29] This analysis is provided in more detail in the Discussion.

One-electron oxidation of **1-CH_2** and **1-C_2H_4** produced a single new absorption at 775 nm (see Figure 7). Similarly, **1-POPh** and **1-PSPh** produced new absorptions at 710 and 760 nm, also with good isosbestic points (see Figure 8). In contrast, the chalcogenides **1-S** and **1-Se** exhibited longer wavelength absorptions, with λ_{max} values of 1090 and 1070 nm, respectively (Figure 9).

Finally, for the purposes of comparison, the radical cation spectra of **1-Ø** and **1-C_2H_2**, previously reported by Spangler and co-workers,[20] were recorded (Figure 10). These are essentially identical with those reported.

Crystal Structures. Single crystals of the linear hydrocarbon and heteroatom-incorporated molecules proved to be very difficult to obtain. Aside from that, relatively low solubility (e.g., $Fc(CH{=}CH)_2Fc$ and $Fc(CH{=}CH)_3Fc$), poor solid morphology due to stereoisomeric mixtures (e.g., **1-PPh**), and flexible backbones could also account for the poorly organized features for compounds of this kind. For these reasons, (*E*,*E*)-**1-S** and (*Z*,*Z*)-**1-PSPh** were the only linearly bridged compounds providing crystals suitable for X-ray crystallographic analysis. The relevant Fe−Fe distances, both through-bond and through-space, are provided in Table 2, and ORTEP plots are given in Figure 11.

The most remarkable structural feature of the *Z*,*Z* isomer is its pseudo-coplanarity along the conjugation path, including the conjugated rings Cp1 and Cp2 attached to the vinyl groups. The disposition of the two ferrocenes is anti. The phenylene ring attached to the phosphorus atom is nearly perpendicular to the bridging plane and takes a face-to-edge orientation to one ferrocenyl group. This steric arrangement certainly has important consequences in minimizing the steric conflict between the aryl and metallocenyl groups and contributes to the nondistorted conjugation pathway. While most of the bond lengths and angles

(27) Connelly, N. G.; Geiger, W. E. *Chem. Rev.* **1996**, *96*, 877–910.
(28) Sohn, Y. S.; Hendrickson, D. N.; Gray, H. B. *J. Am. Chem. Soc.* **1971**, *93*, 3603–3612.
(29) http://www.mpassociates.gr/software/distrib/science/microcal/pfm.html.

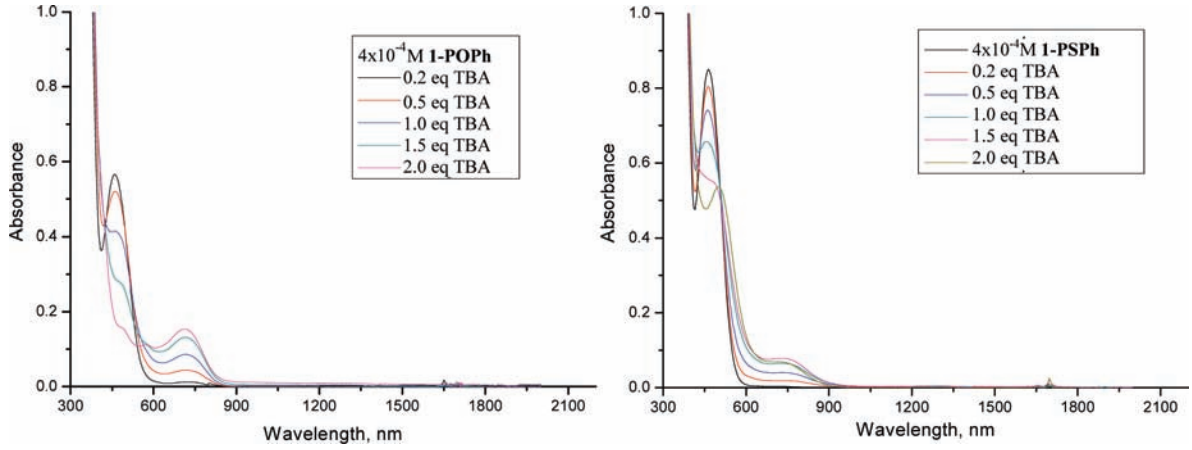

Figure 8. Spectral evolution during one-electron oxidation of **1-POPh** (left) and **1-PSPh** (right).

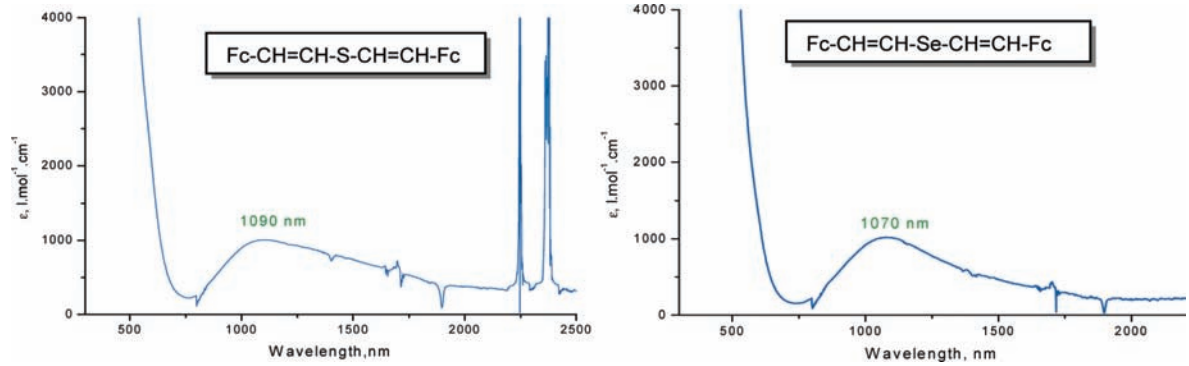

Figure 9. Absorption spectra of the monocationic species of **1-S** (left) and **1-Se** (right).

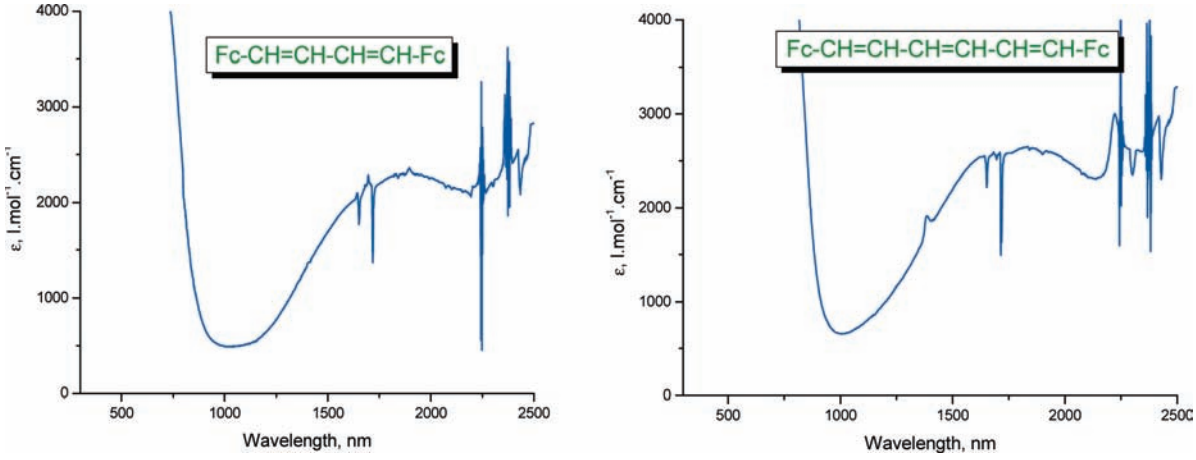

Figure 10. Absorption spectra of the monocationic species of **1-Ø** and **1-C_2H_2**.

Table 2. Selected Steric Parameters for Bis(2-ferrocenylvinyl) Compounds

	1-S	1-PSPh
vinyl,vinyl	*E,E*	*Z,Z*
Fc to Fc	anti	anti
Fe−Fe (space), Å	9.77	9.43
Fe−Fe (bond), Å	13.1	13.3
Cp1-Cp2 (dihedral), deg	52.7	3.16

lie in the normal range, the C(10)−C(11)−C(12) and C(13)−C(14)−C(15) angles are 133.8 and 133.0°, respectively, which helps to maintain coplanarity. In contrast, the C(12)−P(1)−C(13) angle (100.5°) is smaller than expected, resulting in a shorter C(12)−C(13) through-space distance (2.77 Å), analogous to that of **1-S**.

Discussion

Our original objective was to control the conjugation pathway by using a (trans) vinylidene bridge between the ferrocene and the heteroatom to maintain consistency among the various molecules. Although we were unable to obtain sufficient X-ray data to confirm this consistency, it is useful to note that both the through-space and through-bond Fe−Fe distance for **1-S** and **1-PSPh** are almost identical, despite having quite different

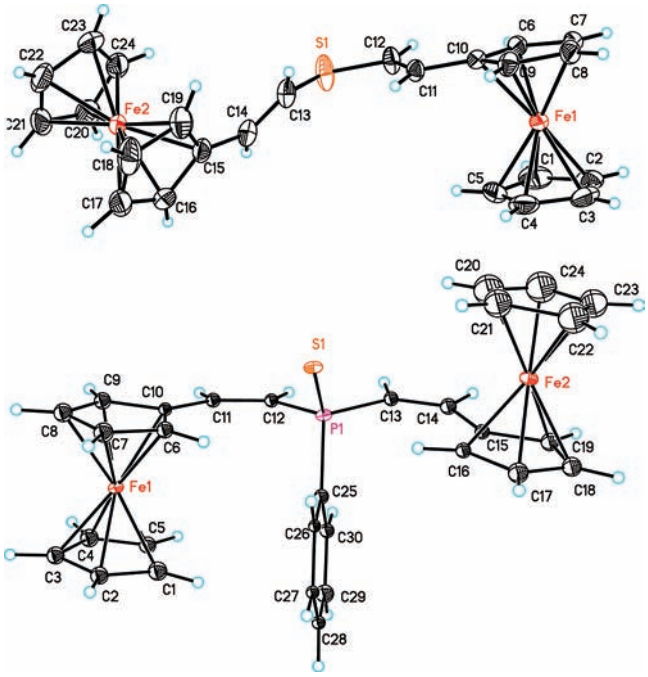

Figure 11. ORTEP plots of (*E*,*E*)-**1-S** (top) and (*Z*,*Z*)-**1-PSPh** (bottom).

couplings. The subject of through-space vs through-bond electronic coupling has been the subject of much study.[30] However, the peak separation (ΔE), which is routinely used to address the degree of electronic coupling between the metal centers, must be a result of a through-bond effect. When no obvious distortion is present in the bridging fragment, the *E*,*Z* configurational difference should play a very small role under such a through-bond mechanism. In this context, it is obviously significant whether we consider distances in terms of metal−metal distances or the ferrocene C atoms at the attachment point. Since ferrocene ground states are characterized by metal-centered HOMOs, we prefer to use the former. This is also consistent with the Hush formalism. Use of the latter would change the distances considered but not the conclusions.

According to the characteristics of their long-wavelength absorptions, the FcCH═CHXCH═CHFc compounds can be divided into two groups: A and B. Group A consists of those molecules (**1-CH$_2$**, **1-C$_2$H$_4$**, **1-PSPh**, **1-POPh**) with short-wavelength (<900 nm) absorptions. These absorptions are very close to the absorptions of ferrocenium itself (675 nm); therefore, we assign those absorptions to a metal-centered interconfigurational (IC) d−d absorption. To deal with the more complex absorptions for the other molecules, we adopt the treatment of Spangler et al.[20] for the hydrocarbon-bridged compounds **1-Ø** and **1-C$_2$H$_2$**. For such mixed-valence species, several absorption bands are observed in the visible and near-IR region, including Cp-to-Fe^{III} charge transfer, bridging ligand $\pi-\pi^*$ transition, bridging ligand to metal charge transfer (LMCT), intervalence charge transfer (IVCT), and the aforementioned IC transition.

In contrast to the simplicity of the visible bands, the absorptions in the near-IR are not straightforward (the vertical lines appearing beyond 2200 nm are from solvent absorption exceeding the compensation capacity of the double-beam spectrophotometer). The broad envelope in the near-IR is deconvoluted using four Gaussians as shown in Figures 12 and 13. The major broad Gaussian component is apparently ascribed to the IVCT transition between the metal centers; the adjacent weak band centered at ca. 8000 cm^{-1} (1250 nm) is assigned to the LMCT derived from the electron transition from the bridging ligand to the Fe^{III} d orbital. Another weak band appearing at higher energy around 10 000 cm^{-1} (1000 nm) was necessary for good spectral fits and has been noticed in other diferrocenyl systems.[20] Unfortunately, the literature is somewhat deficient in this area, because of the fact that nearly all the relevant reports associated with ferrocenium complexes cut the low-energy absorption spectrum at 2200 nm, presumably avoiding the strong solvent interferences depicted above. However, it has been well established that the Ru^{III} and Os^{III} complexes often demonstrate interconfigurational (IC) transition bands derived from the dπ → dπ transitions between the Kramers doublets,[31] as illustrated in Figure 12. The IC bands are nominally parity or LaPorte forbidden but gain intensity through spin−orbit coupling and metal−ligand mixing. They appear in the near-IR (between 4000 to 6000 cm^{-1}) as narrow ($\Delta\varepsilon_{1/2}$ < 1000 cm^{-1}), relatively weak bands,[32] which are almost the same characteristics as the band we observed in the ferrocenium complexes. Therefore, we tentatively assigned this band, centered at 2400 nm, to an IC transition.

While group A includes compounds not showing the IVCT band in the mixed-valence state, group B contains those exhibiting an IVCT transition. The former compounds clearly belong to class I under the Robin−Day classification,[33] which are quasi-insulating systems. For group B compounds, the strengths of electronic coupling could be analyzed from their spectral parameters by the Hush formula[12] (eqs 1 and 2).

Group A includes compounds in which X = P(═O)Ph, P(═S)Ph, CH_2, CH_2CH_2, C═O. It basically contains nearly all of the linearly "interrupted" compounds, which do not have favorable resonance forms for supporting electron transfer. The sample spectra are shown in Figures 8 and 9, where Figure 8 demonstrates the spectral evolution of **1-POPh** and **1-PSPh** upon progressive oxidation with 0.2−2.0 equiv of oxidant. As can be seen, for each mixed-valence species, only a weak low-energy band with λ_{max} falling in the range of ca. 770−1280 nm is revealed, which is assigned to the bridging ligand to Fe^{III} LMCT transition. The spectral data are collected in Table 3. Obviously, the absorption maxima and intensities of the LMCT bands are both associated with the extent of conjugation and electron density on the bridging ligand. Therefore, the LMCT band of **1-S**$^+$ (Figure 9a) appears at the longest wavelength (λ_{max} 1275 nm) with the greatest intensity (ε_{max} = 1750 L M^{-1} cm^{-1}) due to the longest conjugation in this series. In contrast, the corresponding ε_{max} of **1-POPh**$^+$ is very low (300 L M^{-1} cm^{-1}), due to the low electron density on the bridging ligand caused by the electron-withdrawing P═O group (Table 3). For each case of the group A compounds, except the LMCT band, no additional absorption, i.e. an IVCT band, is observed in the near-IR, which implies that this group of compounds has rather insulating bridges. This conclusion seems inconsistent with the electrochemical results, where most of the compounds demonstrated a peak separation, implying the existence of electronic

(30) Sun, D.-L.; Rosokha, S. V.; Lindeman, S. V.; Kochi, J. K. *J. Am. Chem. Soc.* **2003**, *125*, 15950–15963.

(31) (a) Sen, J.; Taube, H. *Acta Chem. Scand., Ser. A* **1979**, *33*, 125–135. (b) Hill, N. J. *J. Chem. Soc., Faraday Trans. 2* **1972**, *68*, 427–434.

(32) (a) Demadis, K. D.; El-Samanody, E.-S.; Coia, G. M.; Meyer, T. J. *J. Am. Chem. Soc.* **1999**, *121*, 535–544. (b) Kober, E. M.; Goldsby, K. A.; Narayana, D. N. S.; Meyer, T. J. *J. Am. Chem. Soc.* **1983**, *105*, 4303–4309.

(33) Robin, M. B.; Day, P. *Adv. Inorg. Chem. Radiochem.* **1967**, *10*, 247–422.

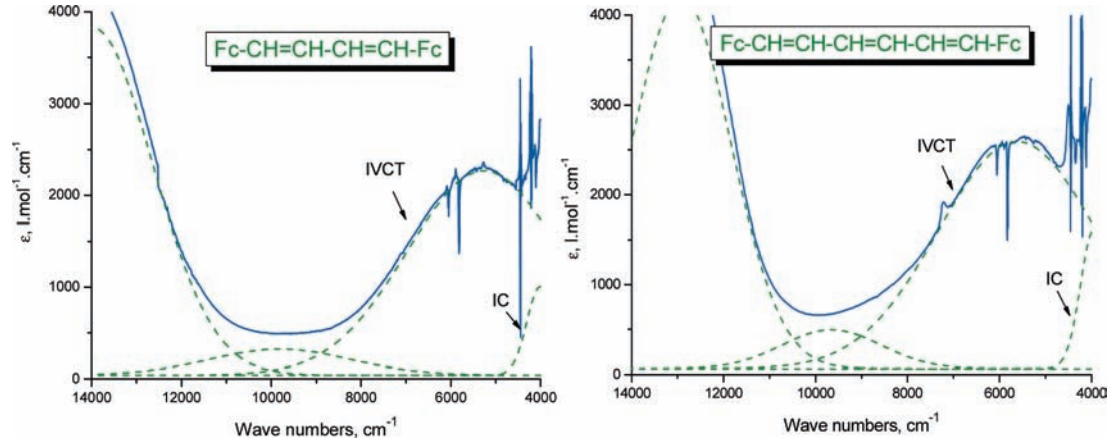

Figure 12. Deconvoluted spectra of (a) $Fc(CH{=}CH)_2Fc^+$ (b) and $Fc(CH{=}CH)_3Fc^+$.

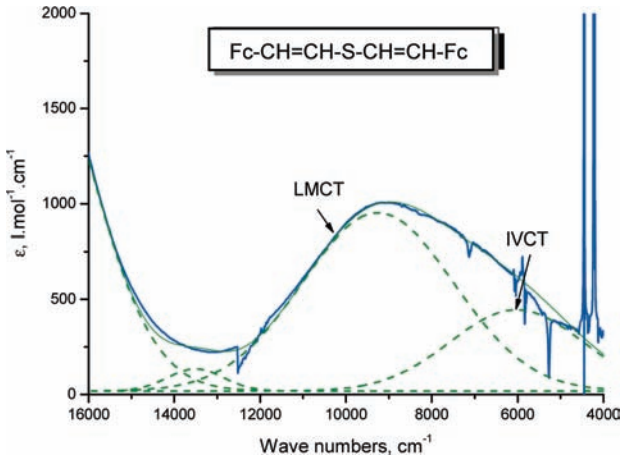

Figure 13. Spectral decomposition of the **1-S**$^+$ absorption spectrum.

Table 3. LMCT Band Parameters, Obtained from the Spectral Deconvolution, of the Mixed-Valence Species of Group A Compounds

compd	ν_{max}, cm^{-1}	λ_{max}, nm	ε_{max}, M^{-1} cm^{-1}	$\Delta\nu$, cm^{-1}
$[\mathbf{1\text{-}CH_2}]^+$	12 850	778	420	3020
$[\mathbf{1\text{-}C_2H_4}]^+$	12 850	778	420	3020
[1-POPh]$^+$	13 980	715	300	2630
[1-PSPh]$^+$	13 430	745	230	2670

coupling. However, it is important to realize that interpretation of ΔE data is less straightforward than that of IVCT data because the former depends on stabilizing factors in the Fe^{II}/Fe^{II}, Fe^{II}/Fe^{III}, and Fe^{III}/Fe^{III} species, on through-space electrostatic and through-bond inductive effects, and on solvation.[34] The lack of IVCT band in the mixed-valence species above suggests that there is no intrinsic correlation between ΔE value and intervalence transition.

In addition to **1-S** and **1-Se**, group B also includes compounds in which X = "-", CH=CH, i.e., systems with π conjugation. The mixed-valence spectra for the latter are shown in Figure 12, and the spectroscopic data obtained after spectral deconvolution are gathered in Table 4. $Fc(CH{=}CH)_2Fc$ (**1-Ø**) and $Fc(CH{=}CH)_3Fc$ (**1-C_2H_2**) have been previously studied by Spangler and co-workers.[20] The reported results are also included in Table 4. In comparison with the literature, our current data present two major differences, which we associate with the different experimental conditions used in developing and measuring the mixed-valence species: i.e., spectroelectrochemical[20] and chemical (this work) oxidation. First, the IVCT ν_{max} (or λ_{max}) values of the current results are shifted (ca. 300 cm^{-1}) to lower energy. It is well-known that, according to Marcus theory for outer-sphere electron transfer,[11b,35] the IVCT bands can be altered significantly by external factors such as solvent, ion pairing, concentration of counterion, temperature, etc. That is, $\lambda_{IVCT} = \lambda_{in} + \lambda_{out}$, where λ_{in} and λ_{out} are the inner- and outer-sphere reorganization energies in the light-induced electron transfer process, respectively. Most likely, the red shifts of the current IVCT bands come from the low concentration of PF_6^- (ca. $1-3 \times 10^{-4}$ M, essentially the same as that of the mixed-valence species) present, in comparison to the high concentration of counterion (0.1 M $Bu_4N^+PF_6^-$) used in electrospectroscopic measurements. Second, the calculated ε_{max} of IVCT is at least 25% greater than the literature result due to the advantages of chemical oxidation over electrochemical oxidation in moderating the underestimation of ε_{max} as discussed earlier. This in turn contributed to the higher V_{ab} and α values.

Interestingly, the mixed-valence absorption of **1-S**$^+$ in the near-IR (Figure 9) is much broader than a normal LMCT band. Whereas the predominant absorption centered at ca. 1090 nm is clearly ascribed to a LMCT transition, there is a noticeable band buried by the tailing segment of the LMCT band, which indeed possesses the IVCT feature upon spectral deconvolution. Although this IVCT band is relatively weak in terms of both intensity (ε_{max} = 440 L M^{-1} cm^{-1}) and calculated electronic coupling constant (V_{ab} = 202 cm^{-1}), it is the first example demonstrating that a heteroatom can also serve as the supporting element for electron transfer in the context of a photodriven process. Thus, **1-S** belongs to group B. On the basis of this, we expect that **1-PPh**$^+$ and **1-O**$^+$ should also present IVCT bands similar to that of **[1-S]**$^+$, since both compounds showed even greater ΔE values in electrochemistry. Unfortunately, these two mixed-valence species are chemically unstable, and no absorptions could be observed in the low-energy area.

Finally, it is worth mentioning that the appearance, band shape, absorption maximum, and intensity of all the bands discussed above are very case-dependent for the series of mixed-valence species herein. The IVCT transition is of the most interest, since it provides the spectral information associated with the strength of the electronic interaction. However, we must caution that the assignments remain somewhat tentative.

(34) Nelsen, S. F.; Trieber, D. A., II; Ismagilov, R. F.; Teki, Y. *J. Am. Chem. Soc.* **2001**, *123*, 5684–5694.

(35) Marcus, R. A. *J. Chem. Phys.* **1965**, *43*, 679–701.

Table 4. IVCT and LMCT Band Parameters, Obtained from the Spectral Deconvolution, and Calculated Hush Parameters for the Mixed-Valence Species of Group B[a] Compounds

compd	ν_{max}, cm^{-1}	λ_{max}, nm	ε_{max}, M^{-1} cm^{-1}	$\Delta\nu$, cm^{-1}	R_{mm},[b] Å	V_{ab},[c] cm^{-1}	α[d]
$Fc(CH{=}CH)_2Fc^+$ (**1-Ø**$^+$)	5290	1960	2280	3900	9.21[f]	483	0.091
$Fc(CH{=}CH)_2Fc^{+}$[e]	5500	1820	1570	4340	9.21[f]	430	0.078
$Fc(CH{=}CH)_3Fc^+$ (**1-C_2H_2**$^+$)	5660	1770	2590	4100	11.54[f]	436	0.077
$Fc(CH{=}CH)_3Fc^{+}$[e]	6010	1660	2100	3800	11.54[f]	390	0.065
[**1-S**]$^+$	6020	1660	440	3640	9.78	206	0.034
	9257[g]	1080	965	4176			0.034
[**1-Se**]$^+$	5270	1900[b]	160	4200	*h*	*h*	
	9265[g]	1079	990	4330			

[a] See text. [b] Spatial iron−iron distance obtained from the crystal structure if not otherwise stated. [c] Hush coupling constant $V = (2.06 \times 10^{-2})(\varepsilon_{max}\Delta\nu_{1/2}\nu_{max})^{1/2}/R_{mm}$. [d] Delocalization efficient $\alpha = V_{ab}/\nu_{max}$. [e] Obtained from ref 20. [f] Obtained from theoretical calculations. [g] LMCT transition as described in text. [h] Not determined.

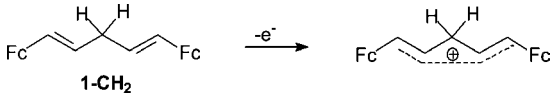

Figure 14. Homoconjugation in **1-CH_2**$^+$.

With these observations, it is possible to discuss the transmission characteristics of the individual moieties X for a charge localized on the end of the molecule. The differences in first and second oxidation potentials, ΔE_{ox}, have often been used as measures of the attenuation factor. As Nelsen has pointed out, such measures can be complicated by screening due to solvation.[34] Indeed, we ourselves have observed a significant difference in ΔE as a function of counterion, and we cannot conclude that the BArF group leads to elimination of solvation effects on the cation. Thus, the ΔE_{ox} we obtain may be attenuated by such effects. Nevertheless, within this approximation, ΔE_{ox} becomes a first-order measure of that attenuation factor (see Table 1). For instance, lengthening the chain from butadiene (**1-Ø,** $\Delta E_{ox} = 225$ mV) to hexatriene (**1-C_2H_2**, $\Delta E_{ox} = 180$ mV) reduces the coupling by 45 mV, while an ethane bridge (**1-C_2H_4**) reduces the coupling to 0. In contrast, a triple bond (**1-C_2**, $\Delta E_{ox} = 1250$ mV) has a 100 mV attenuation and thus is a much poorer coupling moiety. Similarly, a C═O group, while increasing both oxidation potentials, maintains a significant coupling, suggesting simple mixing of lower-lying orbitals may not be a significant factor. Somewhat surprisingly, the methylene bridge (**1-C_2H_2**, $\Delta E_{ox} = 115$ mV) retains significant coupling. This molecule is reminiscent of "interrupted" polyacetylene[36] and suggests that some homoconjugation is possible for the radical cation (see Figure 14).[37]

For heteroatoms, we see that oxygen (**1-O,** $\Delta E_{ox} = 180$ mV) retains the most coupling, diminishing in the order O < S < Se, with oxygen having somewhat better transmission characteristics than a double bond, while sulfur is equivalent to a double bond and the carbonyl group is equivalent to a triple bond. Phosphorus, in contrast, overlaps these two groups, with a modest preference for the phosphine sulfide. We suspect that high-level calculations are required to unravel this distinction. Again, we cannot distinguish the effect of the heteroatom itself from its associated solvation shell, but we do not expect the latter to change this order, given the subtle differences in structure among the various diferrocenes.

The near-IR absorption wavelengths mirror these trends. Molecules with significant IVCT bands show high transmission characteristics, although oxygen and sulfur, with only LMCT charge-transfer characteristics, are also effective. We associate the presence of an IVCT band with a superexchange mechanism, while the LMCT band indicates the presence of a discrete ligand-centered radical-ion state and the possibility of hopping. In the latter case, oxidation of the iron center is a dynamic process which our electrochemical measurements cannot resolve.

Conclusions

These studies present validation for the use of sulfur as an electrically equivalent moiety for charge transport in unsaturated chains, although oxygen has superior transmission characteristics, presumably because of its readily accessible 2p electrons. In contrast, the triple bond exhibits a severe attenuation, which makes its extensive use in molecular wires problematic. In a forthcoming paper, we will examine the role of aromatic and heteroaromatic rings in such systems.

Acknowledgment. We thank the U.S. Department of Energy through Grant No. FG05-85ER45194 for continuing financial support.

Supporting Information Available: Text giving experimental information, including synthetic details, characterization data, and details of spectroscopic manipulations and acquisition, and CIF files giving crystallographic data for (*E*,*E*)-**1-S** and (*Z*,*Z*)-**1-PSPh**. This material is available free of charge via the Internet at http://pubs.acs.org.

JA101585Z

(36) Surjan, P. R.; Kuzmany, H. *Phys. Rev. B: Condens. Matter Mater. Phys.* **1986**, *33*, 2615–24.

(37) For leading references, see: (a) Paddon-Row, M. N.; Shephard, M. J.; Jordan, K. D. *J. Phys. Chem.* **1993**, *97*, 1743–1745. (b) Weng, H.; Du, X.-M.; Roth, H. D. *J. Am. Chem. Soc.* **1995**, *117*, 135–140.